technologies

MDPI

Article

Numerical Simulations of Thermodynamic Processes in the Chamber of a Liquid Piston Compressor for Hydrogen Applications

Valerijs Bezrukovs [1], Vladislavs Bezrukovs [1], Marina Konuhova [1,2], Deniss Bezrukovs [1], Imants Kaldre [3] and Anatoli I. Popov [2,*]

[1] Engineering Research Institute, Ventspils International Radio Astronomy Centre, Ventspils University of Applied Sciences, LV-3601 Ventspils, Latvia; elmag@inbox.lv (V.B.); vladislavsb@venta.lv (V.B.); marina.konuhova@cfi.lu.lv (M.K.); dbezrukovs@gmail.com (D.B.)
[2] Institute of Solid State Physics, University of Latvia, 8 Kengaraga, LV-1063 Riga, Latvia
[3] Faculty of Physics, Mathematics and Optometry, University of Latvia, LV-1004 Riga, Latvia; imants.kaldre@lu.lv
* Correspondence: popov@latnet.lv

Abstract: This paper presents the results of numerical simulations examining the thermodynamic processes during hydraulic hydrogen compression, using COMSOL Multiphysics® 6.0. These simulations focus on the application of hydrogen compression systems, particularly in hydrogen refueling stations. The computational models employ the CFD and heat transfer modules, along with deforming mesh technology, to simulate gas compression and heat transfer dynamics. The superposition method was applied to simplify the analysis of hydrogen and liquid piston interactions within a stainless-steel chamber, accounting for heat exchange between the hydrogen, the oil (working fluid), and the cylinder walls. The study investigates the effects of varying compression stroke durations and initial hydrogen pressures, providing detailed insights into temperature distributions and energy consumption under different conditions. The results reveal that the upper region of the chamber experiences significant heating, highlighting the need for efficient cooling systems. Additionally, the simulations show that longer compression strokes reduce the power requirement for the liquid pump, offering potential for optimizing system design and reducing equipment costs. This study offers crucial data for enhancing the efficiency of hydraulic hydrogen compression systems, paving the way for improved energy consumption and thermal management in high-pressure applications.

Keywords: hydrogen; refueling stations; hydraulic compressors; numerical simulations; COMSOL; heat transfer; CFD modeling; energy efficiency

Citation: Bezrukovs, V.; Bezrukovs, V.; Konuhova, M.; Bezrukovs, D.; Kaldre, I.; Popov, A.I. Numerical Simulations of Thermodynamic Processes in the Chamber of a Liquid Piston Compressor for Hydrogen Applications. *Technologies* **2024**, *12*, 266. https://doi.org/10.3390/technologies12120266

Academic Editors: Dongran Song, Xavier Fernando, Pratheepa Jeganathan and Nades Palaniyar

Received: 27 October 2024
Revised: 7 December 2024
Accepted: 16 December 2024
Published: 18 December 2024

1. Introduction

Hydrogen is one of the most abundant elements on Earth [1], and it has recently gained significant attention as a key element in addressing climate change and transitioning to clean energy. Its potential to decarbonize sectors that are hard to electrify, such as industry and transportation, makes it a promising energy source for the future [2]. Hydrogen can also be used for energy storage from renewable sources, helping to address the intermittency of these sources [3]. At the same time, the European Union has set an ambitious goal to become the first climate-neutral continent by 2050, which is in line with the guidelines of the European Commission, further emphasizing the importance of hydrogen in achieving these sustainability targets [4].

The growing role of hydrogen energy in a sustainable future highlights the importance of addressing safety concerns for both the scientific community and industry [5–7]. Analysis of the current state of research reveals the main key challenges and future directions. Over the past decades, interest in the issues of hydrogen storage, combustion, and spontaneous ignition has grown significantly, indicating their increasing importance [8–13]. Nevertheless,

the use of hydrogen is associated with high costs, as well as challenges in production, storage, and transportation. The lack of infrastructure also limits its widespread adoption [14].

Transitioning to a hydrogen-centric energy landscape requires integrating knowledge from various fields, such as geochemistry, biology, and engineering, paving the way for a sustainable and environmentally friendly future [3]. Compressed, liquid, and cryo-compressed hydrogen provide high efficiency due to their high volumetric and gravimetric density, making them attractive for compact storage [15]. The development of new storage systems, improved infrastructure, and integration technologies is crucial for realizing the full potential of hydrogen as a clean energy source [16,17]. Among compression technologies, liquid piston compression systems stand out for their unique advantages.

Hydrogen is poised to play a central role not only in energy generation but also in various applications, such as electric mobility and industrial processes. Electric mobility is anticipated to be a key aspect of the energy system's decarbonization, with hydrogen-powered fuel cell electric vehicles (FCEVs) emerging as strong candidates [18,19]. FCEVs offer specific advantages over battery electric vehicles (BEVs), such as longer range and significantly lower refueling times, which make them highly suitable for long-distance travel and commercial applications. These benefits are facilitated by high-pressure hydrogen tanks that can be filled in less than five minutes at dedicated compression storage dispensing (CSD) stations [20]. For hydrogen refueling, establishing the necessary infrastructure is critical [21]. Because of this, hydrogen refueling stations (HRSs) are created. In a hydrogen refueling station, hydrogen is compressed from low pressure (0.1–3.0 MPa) to a high pressure in the range of 35.0 bar to 70.0 MPa and is stored in high-pressure cylinders [22].

Two primary methods for supplying hydrogen to refueling stations include on-site production and transportation-based delivery [23]. When transported via truck, hydrogen is typically stored and transported at high-pressure levels of 25–30 MPa or between storage nodes at 50–54 MPa [24]. However, hydrogen's high diffusivity imposes pressure limitations, leading to potential losses over extended periods at high pressures [25].

Figure 1 illustrates a schematic of a hydrogen refueling station using hydrogen at inlet pressures ranging from 0.6 to 25.0 MPa, delivered either by trailer or generated on-site through electrolysis [26]. This approach is particularly appealing when coupled with green hydrogen production powered by wind turbines, solar panels, or nuclear energy. Using a booster compressor, low-pressure hydrogen is raised to 70 MPa for cars and 35 MPa for trucks before being stored in high-pressure tanks. From there, hydrogen is dispensed into vehicle fuel tanks via a dispenser.

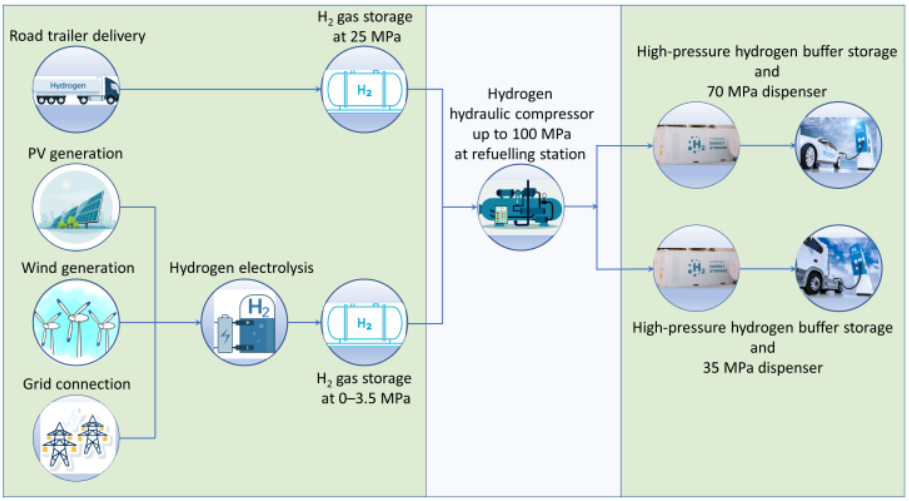

Figure 1. Schematic diagram of the delivery, storage, and preparation of compressed high-pressure hydrogen for use at refueling stations.

Depending on the production method, hydrogen is conventionally labeled green, blue, pink, and grey, and specialized terms like safe, sustainable, low carbon, and pure are also used [27]. The utilization of renewable energy sources, which are practically inexhaustible, for hydrogen generation allows one to establish a continuous, sustainable, and ecologically clean energy production cycle. Thus, "green" hydrogen is one of the most promising approaches for future energy storage infrastructure development projects [28,29].

In green hydrogen production, the focus is on utilizing wind and solar energy [30,31]. Modern technological advancements allow for hydrogen production via water electrolysis without carbon dioxide emissions, ensuring the process remains carbon-free when powered by renewable or nuclear electricity [32]. Thus, the entire process of water electrolysis and hydrogen generation can potentially be carbon-free if renewable or nuclear electricity is used.

Deploying hydrogen infrastructure for vehicle refueling requires simple and cost-effective solutions for hydrogen compression. Recent studies [32] have reviewed existing hydrogen compression technologies, highlighting their operating principles, advantages, and limitations. Among these, liquid piston compressors are particularly notable for their ability to achieve quasi-isothermal compression with minimal energy consumption [33].

This efficiency is driven by the rapid heat exchange between the liquid piston and the gas during compression, promoting near-isothermal operation. Numerical modeling studies confirm their advantages, demonstrating hydraulic compression from 1.5 MPa to 45 MPa in a 31.72 L chamber [34]. These systems also address challenges like gas leakage and mechanical wear, enhancing their potential for advancing hydrogen infrastructure.

The liquid piston compression concept uses a column of liquid to directly compress gas in a fixed-volume chamber [35]. After the compression stroke, the heated liquid is directed to a heat exchanger for cooling, eliminating the need for external heat exchangers on the chamber [36]. Studies have shown that liquid piston compressors can improve efficiency from 70% to over 84–86% [37], but challenges in optimizing heat transfer and thermodynamic processes remain.

The efficiency of liquid piston compressors depends heavily on effective heat transfer. Inadequate heat dissipation can lead to increased energy consumption, mechanical stress, and reduced system longevity [38]. Research highlights the need for improved modeling of heat transfer processes, particularly under dynamic compression conditions involving temperature and pressure fluctuations [39–43].

Heat transfer processes within the compressor cylinder are critical for determining system efficiency and performance. These processes influence the thermodynamic cycle by affecting compression temperature and energy consumption. Inadequate heat dissipation or improper modeling can lead to higher temperatures, increasing the energy required for compression and reducing efficiency. Excess heat can also cause mechanical stress and component wear, leading to higher maintenance costs and shorter equipment lifespans.

Increasing heat transfer coefficients at interfaces and within walls, along with extended compression time, reduces hydrogen temperatures by enhancing thermal energy dissipation. An accurate modeling of these processes under dynamic conditions, including temperature and pressure fluctuations, is vital for optimizing cooling systems and minimizing energy losses. While these principles are well established, numerical simulations quantify their impact, validating the model's practical applicability and guiding the design of efficient, cost-effective compression systems.

The authors in [44] noted the complexity of heat transfer processes within liquid piston compressors, especially under transient and turbulent regimes. Numerical modeling has been used to simulate single compression strokes and study heat transfer phenomena in compression chambers [45]. Thermal analyses of liquid piston compressors have focused on systems with small pressure ratios, while studies involving high-pressure ratios remain limited [46]. Further exploration of these processes through advanced computational models will provide deeper insights into improving system performance.

Numerical and experimental studies have provided valuable insights into these challenges. Computational Fluid Dynamics (CFD) tools, such as COMSOL Multiphysics® [47], have been used to validate thermodynamic models and enhance the understanding of compression dynamics [48]. Innovations, such as incorporating porous media within the chamber, have demonstrated significant improvements in heat dissipation and compression efficiency [49,50].

The interplay between chamber geometry and hermodynamicc processes has driven recent advancements in compressor design [36,51–53]. These developments have led to a new generation of hydraulic compressors optimized for hydrogen production chains involving electrolysis, storage, and dispensing at fueling stations. However, gaps remain in understanding long-term thermal effects in multi-cycle operations, such as heat accumulation in chamber walls and working fluid. Addressing these issues through advanced numerical models and experimental validation will enable the development of robust hydrogen compression systems suitable for practical applications.

The paper Is organized as follows. Section 2 describes the numerical modeling approach used to analyze hydrogen compression in a closed cylindrical chamber. Section 3 focuses on the hydrogen compression process, evaluated using COMSOL 6.0 to study the effects of chamber dimensions and compression rates on thermodynamic processes. Section 4 presents simulation results, including energy costs, power consumption, and temperature increases in the gas, oil, and chamber walls. Section 5 provides the conclusions.

2. Modeling of Hydraulic Hydrogen Compression

The modeling of hydrogen hydraulic compression is a crucial aspect of understanding and optimizing the thermodynamic processes involved in the compression of hydrogen, particularly within a hydraulic compression system [54,55]. Modeling provides valuable insights into the behavior of hydrogen under high-pressure conditions, which is especially important for designing efficient and safe hydrogen storage and transport systems. Hydraulic compression systems are often used to compress hydrogen due to their ability to achieve high pressures while maintaining control over the thermodynamic states of the gas. The accurate modeling of these processes helps engineers and researchers predict how hydrogen will behave during compression, including temperature and pressure changes, heat generation, and heat transfer to the surrounding materials.

One of the key benefits of numerical modeling is that it allows for the simulation of various scenarios, such as different compression speeds, chamber geometries, and fluid properties, without the need for costly and time-consuming physical experiments. This provides a deeper understanding of how the system will respond to changes, enabling a better optimization of the compression process. For example, modeling can help to determine how much heat is generated during compression and how effectively that heat can be dissipated by the oil and cylinder walls. This knowledge is essential for preventing overheating, improving energy efficiency, and ensuring the longevity of the equipment.

Moreover, the ability to simulate the interaction between the gas, the oil, and the compression chamber walls gives the ability to evaluate how heat transfer affects the final pressure and temperature of the compressed hydrogen. This is particularly important in non-adiabatic processes where heat is lost to the environment or absorbed by the surrounding materials. By understanding these effects, the system can be fine-tuned to minimize energy losses and reduce the amount of work required to achieve a specific compression ratio.

This section outlines the numerical modeling approach employed to analyze hydrogen compression within a closed compression chamber.

The base model is a closed cylindrical chamber with a height (h) of 145.0 mm and an inner diameter (d) of 100.0 mm, resulting in a total volume (V) of 1.14 L (Figure 2). The chamber is made of stainless steel, with a wall thickness (d_{wall}) of 5.0 mm, and is divided into an upper section filled with hydrogen and a lower section filled with an oil. During the compression process, the oil level rises, compressing the hydrogen above it. The numerical

model implemented considers heat exchange between the hydrogen gas, the oil, and the cylinder walls, as well as convective heat transfer to the surrounding environment.

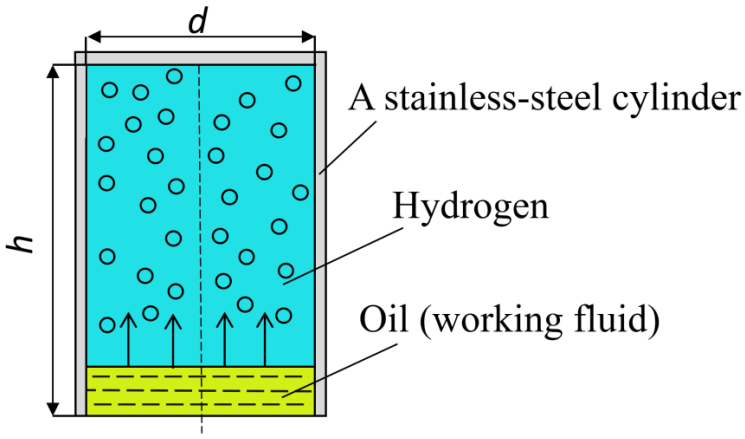

Figure 2. A model of a steel cylinder shaped chamber where hydrogen is compressed by the oil (working fluid) coming from the bottom in the direction of the arrow.

The purpose of the simulation was to examine the temperature variations of hydrogen, the cylinder walls, and the oil, as well as to estimate the actual pressure inside the chamber during the compression process. The pressure increase in the cylinder was modeled as a result of discrete volume changes, achieved by incremental rises in the oil level. The model assumed that properties of the gas and oil are uniformly distributed throughout the compression process, with the time step for discrete volume changes set to Δt_s = 0.01 s.

The physical properties of hydrogen, oil, and the stainless-steel cylinder used in the model are summarized in Table 1. The properties of hydrogen, including molar mass and heat capacity, are taken from [56]. The material properties of stainless steel and oil were obtained from the COMSOL Multiphysics® Material Library [57]. Additionally, the simulation accounts for the compressibility of the liquid to ensure an accurate modeling of the thermodynamic processes.

Table 1. Initial parameters and physical properties of hydrogen, liquid piston, and cylinder used in the model.

Initial parameters used in the simulation.	Initial gas temperature, oil (working fluid), cylinder, and surrounding air: T_i = 300.0 K Initial pressure: P_1 = 3.0, 10.0, 15.0, and 20.0 MPa Volume: V = 1.14 L Gas mass in the cylinder: m_{gas} = 2.74 g (at 3.0 MPa); m_{gas} = 9.24 g (at 10.0 MPa); m_{gas} = 13.86 g (at 15.0 MPa); m_{gas} = 18.48 g (at 20.0 MPa) Heat transfer coefficient (cylinder–air): h = 30.0 W/(K·m^2) Cylinder mass: $m_{cylinder}$ = 2400 g Cylinder wall thickness: d_{wall} = 5 mm		
	Property and its variable used in COMSOL	**Value**	**Unit**
Properties of hydrogen.	Molar mass (M)	2.016	g/mol
	Degrees of freedom (f)	5.0	
	Ratio of specific heat (γ)	1.4	
	Heat capacity at constant volume (C_v)	10,307.5	J/kg·K
	Heat capacity at constant pressure (C_p)	14,429.6	J/kg·K

Table 1. *Cont.*

Properties of the liquid piston (oil).	Thermal conductivity	0.4	W/(m·K)
	Density	918.0	kg/m^3
	Heat capacity at constant pressure	2060.0	J/(kg·K)
	Dynamic viscosity	130.6	Pa·s
	Ratio of specific heats	1.0	
Properties of the stainless-steel cylinder.	Thermal conductivity	45.0	W/(m·K)
	Density	7700.0	kg/m^3
	Heat capacity at constant pressure	800.0	J/(kg·K)

The volume of oil V_{Fj} in the compression chamber after each step was determined by the expression:

$$V_{Fj} = \Delta V_F \, j \tag{1}$$

$$\Delta V_F = \frac{V\left(1 - \frac{1}{K_c}\right)}{t_s} \Delta t_s \tag{2}$$

where V—the total volume of the compression chamber.

ΔV_F—discrete increment in the volume of the oil.

$j = 1, 2, 3 \ldots n$—step number for the discrete increase in the oil volume.

$n = t_s/\Delta t_s$—the total number of steps in one compression stroke.

It should be understood that the gas compression process is accompanied by high heat generation, and the high temperature of the compressed gas has an immediate effect on the oil. In fact, the fluid and the gas are compressed together, but since the fluid has a higher density and a higher heat capacity, the heat generated during compression is effectively absorbed by the fluid and the surrounding walls of the compression chamber.

The gas was compressed at constant velocity from volume V_1 to volume V_2 using the compression ratio $K_C = V_1/V_2 = 5.0$.

In the adiabatic case, the ideal gas equation is as follows:

$$PV = nRT \tag{3}$$

For an adiabatic process,

$$PV\gamma = const, \tag{4}$$

where γ can be calculated as follows:

$$\gamma = \frac{c_p}{c_V} = \frac{f+2}{f}, \tag{5}$$

where

P—pressure.

V—the volume of chamber.

n—gas quantity (mol).

$R = 8.31$ J/(mol·K)—universal gas constant.

T—absolute temperature (K).

γ—the ratio of the heat capacity at constant pressure (C_p) to heat capacity at constant volume (C_v).

f—degrees of freedom of ideal gas ($f = 3$ for monoatomic gas, $f = 5$ for diatomic gas).

t—compression time (s).

v—compression velocity.

In the adiabatic case, if compression is performed from the initial parameters V_1, P_1 and T_1, the final parameters can be calculated using the ideal gas law and the conditions for an adiabatic process:

$$P_1 V_1 = nRT_1, \tag{6}$$

$$P_2 V_2 = nRT_2, \tag{7}$$

$$P_1 V_1^{\gamma} = P_2 V_2^{\gamma}, \tag{8}$$

When heat exchange with the steel cylinder and oil piston is considered, part of the heat is transferred to the oil and steel. Consequently, the final pressure and temperature are lower than in the adiabatic case. The total energy required for compression is also lower than in the adiabatic case due to the reduced final temperature and pressure. Thus, pressure and temperature do not follow the adiabatic law:

$$PV^{\gamma} = const \tag{9}$$

This process is implemented in the numerical model as follows:

1. The compression is divided into 20 to 100 time steps.
2. Within each time step, the process is assumed to be adiabatic.
3. The energy added to the gas is introduced as a volumetric heat source.

The instantaneous power density heating the gas is given by the following:

$$P_w = \frac{\frac{dA}{dt}}{V} = P_0 \left(\frac{V_0}{V} \right)^{\gamma} \pi R^2 \frac{v}{V}, \tag{10}$$

where

P_w—the power.
$\frac{dA}{dt}$—the rate of work, interpreted here as the instantaneous power.
V—the current volume.
P_0 and V_0—initial pressure and volume, respectively.
γ—the adiabatic index (the ratio of heat capacities).
πR^2—the cross-sectional area of the piston.
v—the compression velocity.

3. Numerical Modeling of Hydraulic Compression of Hydrogen in COMSOL

In the context of hydrogen compression, numerical modeling in COMSOL offers several key advantages. It allows for detailed simulations of thermal and fluid behavior, providing valuable insights into the interaction between different materials and physical processes [58,59]. By leveraging its robust numerical solvers and customizable physics modules, COMSOL can accurately model the compression of hydrogen, including heat transfer, pressure distribution, and flow characteristics [60].

The hydrogen compression modeling was carried out using COMSOL Multiphysics® 6.0 software, utilizing the CFD and heat transfer modules to accurately simulate the thermodynamic behavior.

This study uses COMSOL to address critical tasks in hydraulic hydrogen compression, such as predicting temperature distribution, evaluating heat exchange between the gas, fluid, and compression chamber, and estimating energy requirements for various compression ratios. Such simulations are essential for optimizing the design of compression systems, ensuring efficient energy consumption, and improving overall system performance.

The numerical model was constructed under the assumptions that the thermal conductivity of the oil is significantly lower than that of hydrogen and that, during the filling of the compression chamber with the oil, no turbulence or mixing occurs between the media.

The transient heat transfer equation was used in the model to calculate the heat transfer processes:

$$y = \underbrace{\rho C_p \frac{\partial T}{\partial t}}_{internal\ energy} + \underbrace{\rho C_p \vec{u} \cdot \nabla T}_{convection} + \underbrace{\nabla \cdot (-k \nabla T)}_{conduction} \quad (11)$$

where

k—thermal conductivity.
C_p—the specific heat capacity.
$\vec{u}$—the velocity vector.
T—the temperature.
$\frac{\partial T}{\partial t}$—the rate of change of temperature over time.

In the numerical model, the initial height of the liquid column is set as a constant value of 100 mm in the base model to establish the initial conditions and simplify the setup (Figure 3). However, during the compression process, the liquid column height incrementally increases as the liquid piston rises and compresses the gas. This dynamic change in the liquid column height is accounted for in the simulation through discrete volume changes over time.

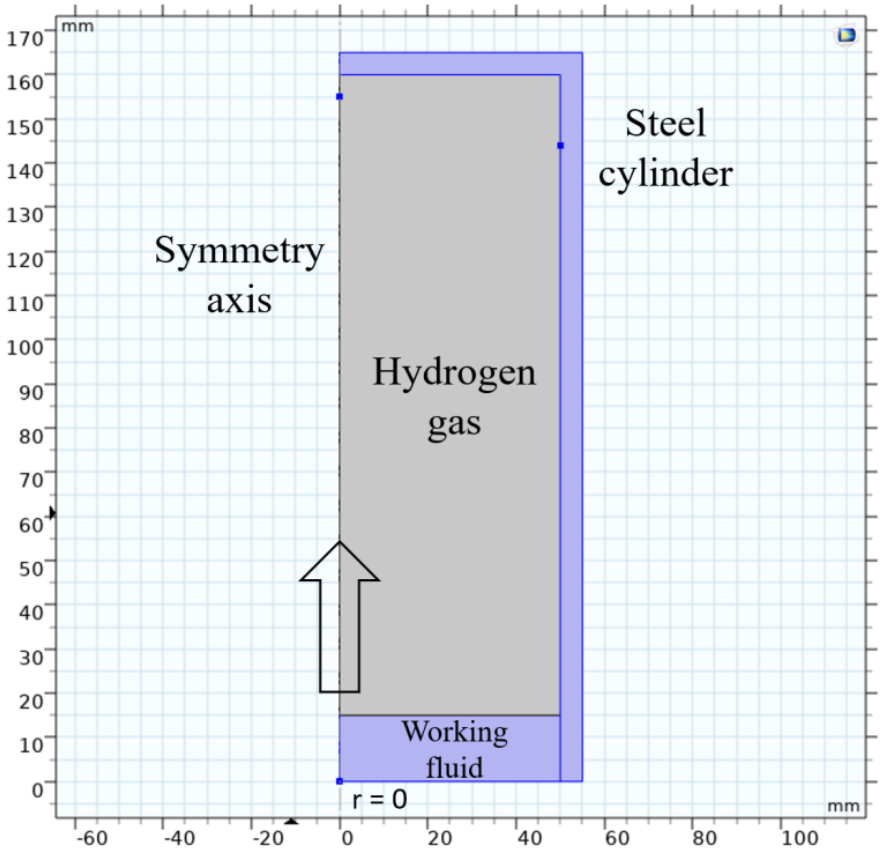

Figure 3. Model of a stainless-steel cylinder chamber for hydrogen compression via fluid injection.

The Deformed Geometry module was used for the gas domain. The mass of the gas was conserved in this domain, and heating, due to the compression of the gas, is introduced as the volumetric heat source, which goes into temperature equation. This model was used prescribed liquid piston motion with constant velocity. To save time in calculating, remesh was not used after every time step; instead, deforming mesh was used, which means that though the same number of cells was conserved, the aspect ratio of the cells changed during the compression process.

An axisymmetric numerical model using a triangular mesh was employed. For accurate calculations of the gas, a relatively coarse mesh is acceptable; however, the boundary layers in the liquid and steel domains require refinement. In the steel cylinder chamber, a maximum mesh element size of 2 mm was used, with a maximum growth rate of 1.2. Boundary refinement consists of 25 layers, applied with a growth rate of 1.005, to ensure an accurate calculation of heat exchange in the contact regions between the oil, hydrogen, and stainless steel.

The boundary condition imposed on the axisymmetric axis includes a no-slip boundary condition for fluid dynamics and a thermal insulation condition for heat transfer. The no-slip condition ensures that the velocity of the fluid along the axis is zero, maintaining no relative motion between the fluid and the axis. The thermal insulation condition sets the heat flux across the axis to zero, consistent with the symmetry assumption that there is no heat transfer through the axis.

The complete mesh comprises 20,909 domain elements and 694 boundary elements.

The position of the liquid piston column in the compression chamber filled with hydrogen, during its upward movement over the stroke time of 0, 10, and 20 s, is shown in Figure 4. As seen in the figure, the volume occupied by hydrogen in the compression chamber decreases, causing a deformation of the mesh cells in this region. Although the number of domain elements remains constant, their density increases. The qualitative changes in the mesh cells of the numerical model at the interface between the media within the compression chamber, as the hydrogen volume decreases to a compression ratio $K_c = 5$ during a single stroke of 20 s, can be seen in Figure 5.

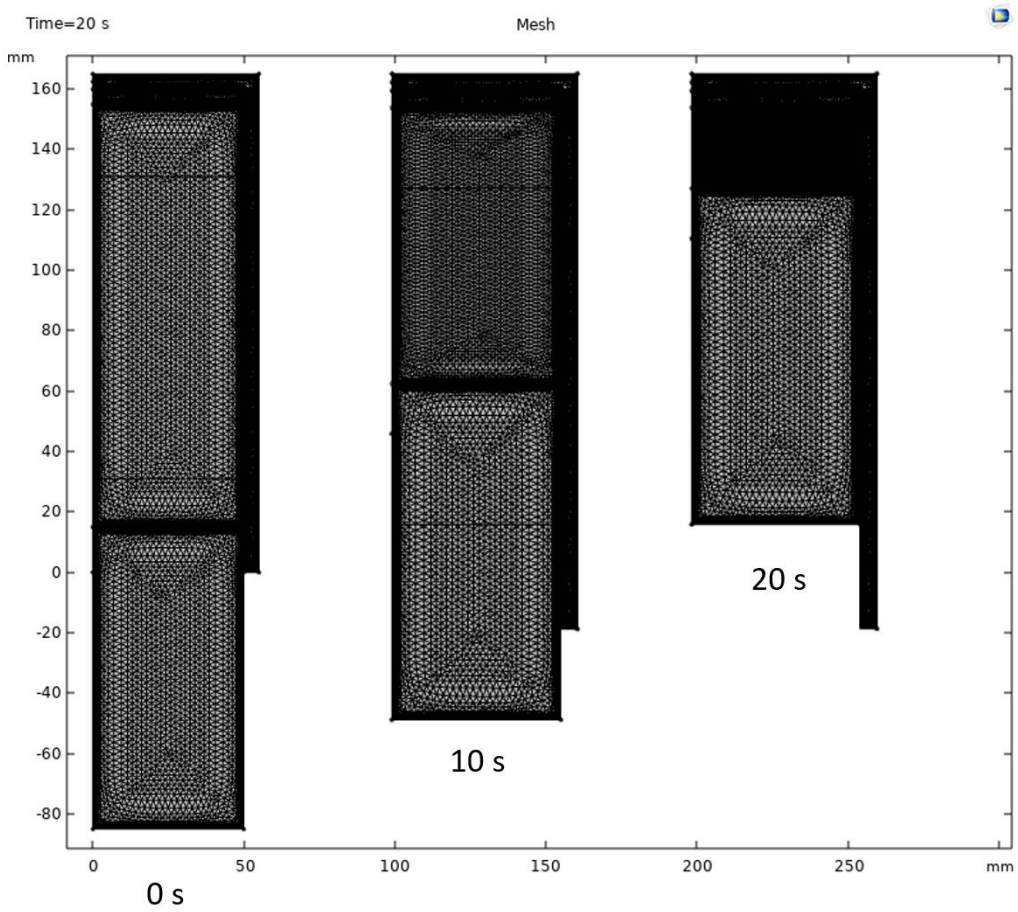

Figure 4. Mesh cell distribution in the numerical model during the change in hydrogen volume within the compression chamber and the position of the liquid piston column as it moves upward at times 0, 10, and 20 s over a single stroke period.

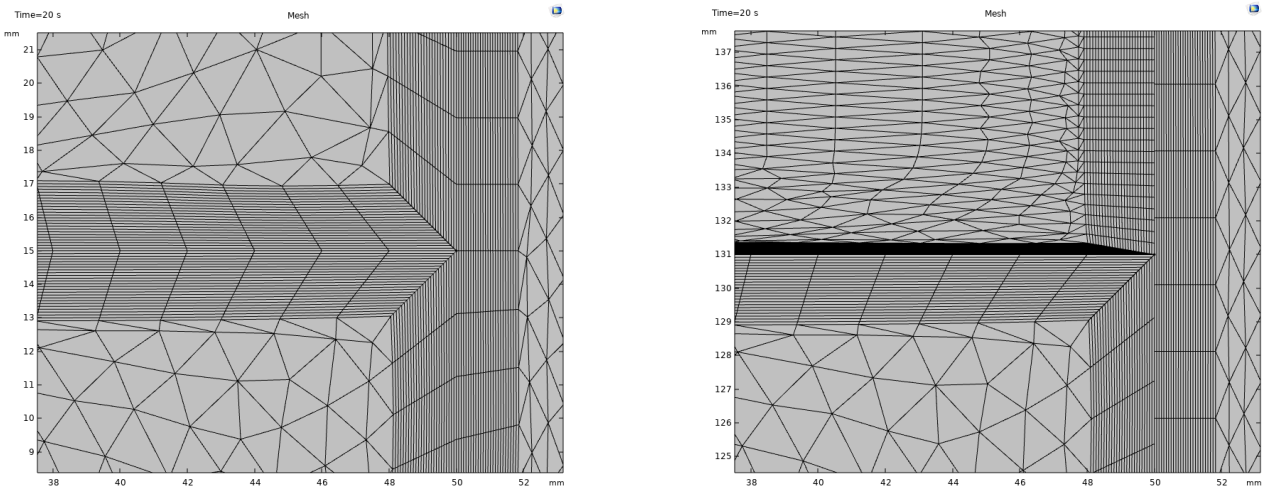

(**a**) (**b**)

Figure 5. The structure of the mesh cells in the numerical model during hydrogen compression in the chamber to a compression ratio K_c = 5.0 for time intervals of (**a**) 0 s and (**b**) 20 s.

In the numerical model, the compression process was divided into multiple small time-steps (0.01 s). The choice of 0.01 s as the time step was based on a balance between computational efficiency and numerical accuracy. Within each discrete time step, the pressure in the gas domain was assumed to remain constant while the temperature was calculated. This simplification facilitates the computational process by focusing on incremental changes. However, over the entire compression stroke, the pressure increases as the gas volume decreases in accordance with thermodynamic principles.

The model provides the temperature distribution in each domain, which can then be averaged by calculating the mean temperature for each domain and the total amount of heat transferred to each domain.

The analysis of the numerical modeling results allows for the investigation of the temperature distribution in the gas medium, oil, and the walls of the compression chamber. Consequently, this enables the estimation of the energy consumption required to achieve a given pressure increase at a specific compression ratio K_c, depending on the compression speed.

To simplify the calculations, the pressure increase within the cylinder chamber was modeled as a result of discrete volume changes, considering both hydrogen and oil, along with the associated rise in gas temperature.

The time step for each discrete change in the oil volume was constant and set at Δt_s = 0.01 s. Each discrete step increases the fluid height by a specific amount, as described by Equation (2), determined by the stroke time t_s. In this model, it is assumed that, at each time step during the hydraulic compression of hydrogen, the properties of both the oil and the gas are uniformly distributed, and their volumes remain unmixed. Heat transfer between the hydrogen, oil, and the walls of the stainless-steel cylinder occurs solely through thermal conductivity of the materials involved.

4. Simulation Results of Hydrogen Hydraulic Compression

Based on the model presented in Section 3, the processes occurring during a single compression stroke, with stroke times t_s ranging from 0.5 to 20.0 s, were simulated. The initial temperature of both the hydrogen and the oil was set to 300 K, with a compression ratio K_c = 5.0. Calculations were performed for two scenarios: one at an initial gas pressure P_1 = 3.0 and another at P_1 = 20.0 MPa.

Figure 6 illustrates the temperature field distributions obtained from the numerical simulations for hydrogen confined within the cylindrical chamber. The figure depicts the temperature evolution of the gas over a 20 s stroke at time intervals of 0, 10, 15, and 20 s. The

color scale corresponds to temperature values ranging from 300 K to 550 K, showing how the gas temperature changes due to compression. These results highlight the significant heating effects within the gas as compression progresses, particularly at higher pressures.

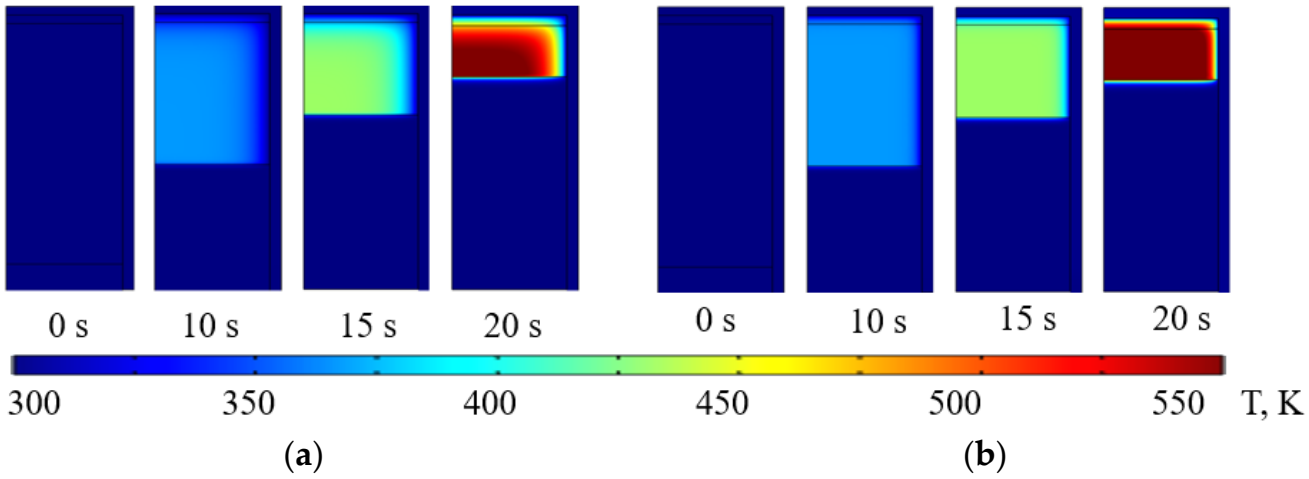

Figure 6. Distribution of the temperature of hydrogen in the compression chamber during a single 20 s compression stroke: (**a**) the initial pressure 3.0 MPa, (**b**) the initial pressure 20.0 MPa.

Figure 7 presents examples of temperature field distributions obtained from numerical simulations for the cylinder walls. The figure illustrates the changes in wall temperature during a 20 s compression stroke, shown at time intervals of 0, 10, 15, and 20 s. The color scale corresponds to temperature values between 300 K and 310 K, demonstrating the relatively minor temperature increase in the cylinder walls compared to the gas, which highlights the effective heat transfer between the gas and the surrounding material during compression.

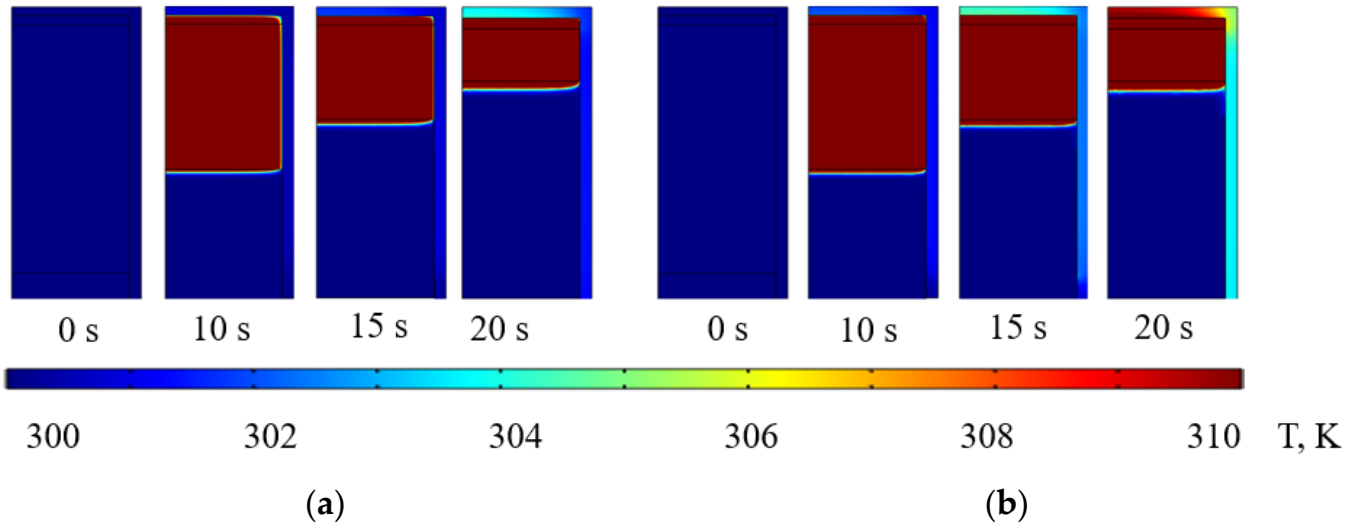

Figure 7. Temperature distribution in the compression chamber wall during a single 20 s compression stroke: (**a**) initial pressure of 3.0 MPa, and (**b**) initial pressure of 20.0 MPa.

The temperature field distribution in the compression chamber, calculated using the superposition method, is crucial for identifying areas where the thermodynamic processes of hydrogen compression generate maximum heat. Understanding the temperature distribution in the cylinder body is particularly important as it directly informs the design of an efficient cooling system to dissipate heat during the compression process.

In this study, the "superposition method" is employed as a numerical approach to simplify the analysis of thermodynamic processes during hydraulic hydrogen compression. This method involves dividing the compression cycle into discrete, incremental steps, with each step representing a small volume change. For each step, the temperature and energy distributions are calculated separately for the gas, the working fluid, and the chamber walls. The results from these discrete steps are then aggregated to provide a comprehensive understanding of the system's behavior over the entire compression process.

The superposition method is particularly advantageous as it enables the efficient modeling of complex, coupled heat transfer and compression dynamics without significantly increasing computational demands. By breaking down the process into manageable increments, this approach ensures accuracy and clarity in representing the thermodynamic interactions within the system.

Figures 6 and 7 reveal that the upper part of the chamber undergoes the most intense heating during compression. Therefore, to optimize the cooling of hydrogen, it is recommended to design the cylinder body with a closed top, maximizing the surface area exposed to external cooling mechanisms, such as air or liquid cooling. This design approach would enhance the heat removal process and ensure the stability of the compression system.

The results of the compression process simulation allow for estimating the temperature rise in the gas and oil and, consequently, determining the energy expended during the hydraulic compression process. In this context, it is important to examine how the compression process is affected by variations in the duration of the compression stroke t_s and the initial hydrogen pressures P_1. Figures 8–10 show how the average temperatures of hydrogen ΔT_H, oil ΔT_F, and steel cylinder ΔT_C change during a single compression stroke, with stroke times t_s ranging from 0.5 to 20.0 s, depending on initial pressure P_1 = 3.0, 10.0, 15.0, and 20.0 MPa.

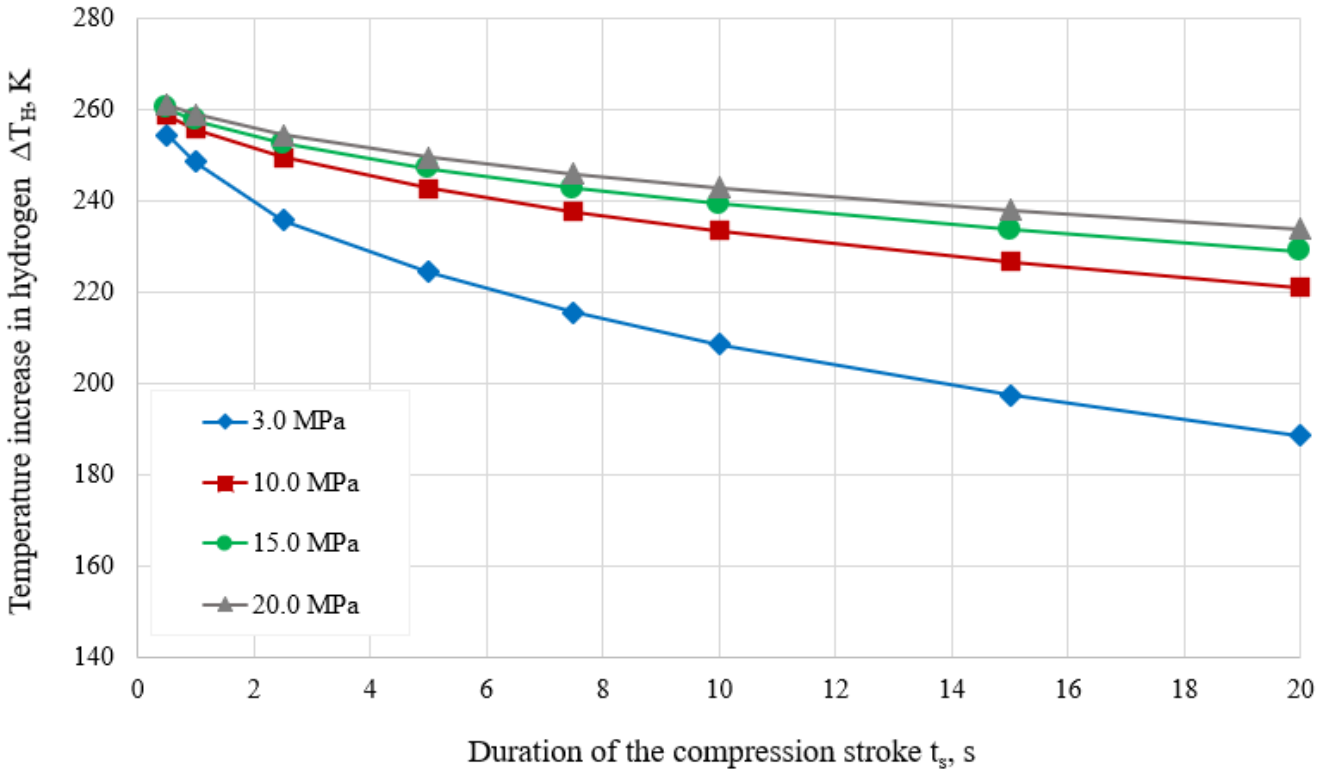

Figure 8. Average temperature increases in hydrogen ΔT_H for different durations of the compression stroke t_s at initial pressures P_1 = 3.0, 10.0, 15.0, and 20.0 MPa and compression ratio K_c = 5.0.

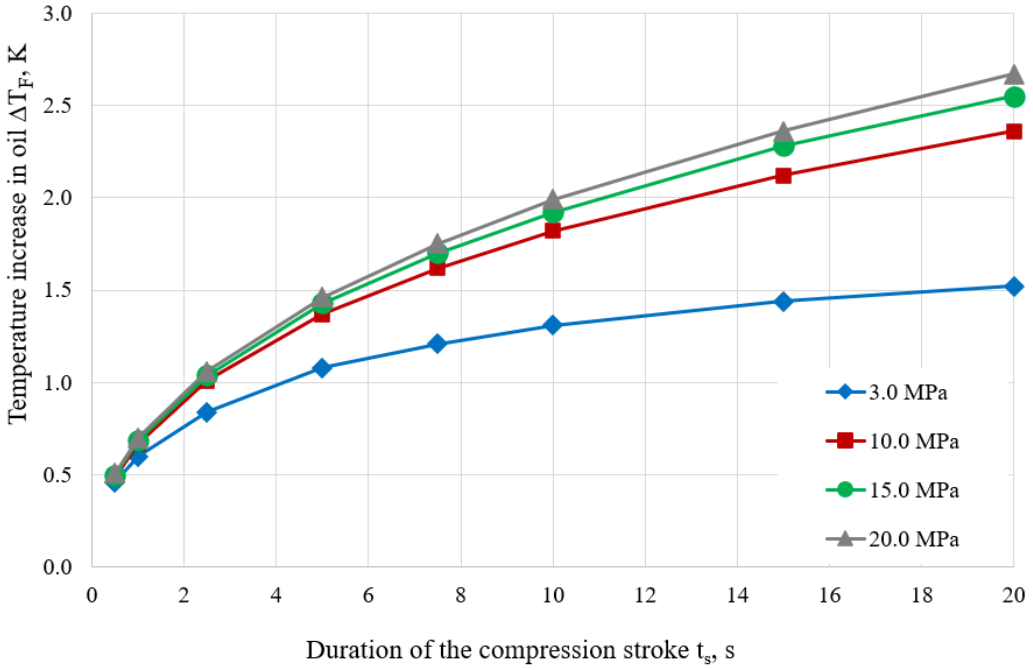

Figure 9. Average temperature increases in oil ΔT_F for different durations of the compression stroke t_s at initial pressures P_1 = 3.0, 10.0, 15.0, and 20.0 MPa and compression ratio K_c = 5.0.

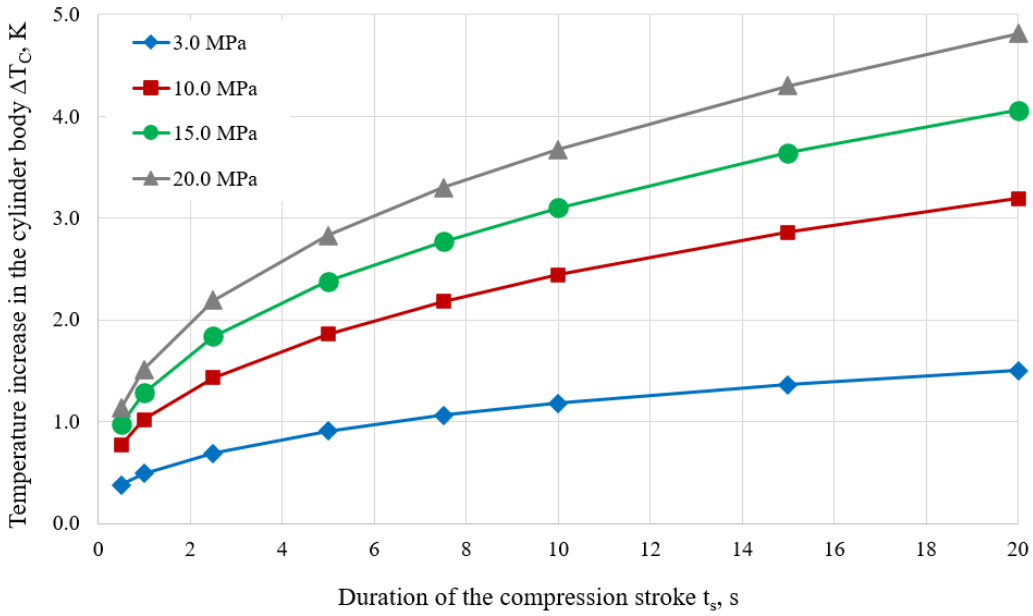

Figure 10. Average temperature increases in the cylinder body ΔT_C for different durations of the compression stroke t_s at initial pressures P_1 = 3.0, 10.0, 15.0, and 20.0 MPa and compression ratio K_c = 5.0.

The increase in temperature values, previously determined in the model, corresponds to the energy involved in the process of the hydraulic compression of hydrogen and accumulated in the hydrogen volume, oil, and cylinder body. The amount of energy stored in the compressed hydrogen, the oil, and the stainless-steel walls of the cylinder is determined using an equation based on the laws of thermodynamics:

$$Q = m\ c\ \Delta T \tag{12}$$

where

m—mass, kg.

c—specific heat capacity, J/(kg·K).

ΔT—the total temperature increase in the medium at the end of the compression stroke, K.

The heat capacity values for hydrogen, the oil, and the stainless-steel cylinder were provided in Table 1. The model accounts for the change in hydrogen mass as the initial pressure increases.

The distribution of total energy Q_T between the oil, hydrogen, and stainless-steel cylinder body is shown for different durations of the compression stroke t_s. The initial hydrogen pressures are P_1 = 3.0 and 20.0 MPa, with the compression ratio set to K_c = 5.0. It can be noted that with raising inlet pressure up to 20.0 MPa most of the energy is concentrated in hydrogen as its mass increases with increasing pressure.

The modeling of the compression process with the use of a superposition method allows us to represent temperature and volumes of energy separately for each medium. Thus, the distribution of the amount of energy Q_T that is spent for the compression process without taking into account losses on convection, between the oil, hydrogen, and steel of the cylinder body depending on the duration of compression cycle t_s, can be presented in the form of a graph shown in Figures 11 and 12. The structure of the energy distribution for initial pressures P_1 = 3.0 and 20.0 MPa and the compression ratio K_c = 5.0 shows that most of the energy is concentrated in hydrogen.

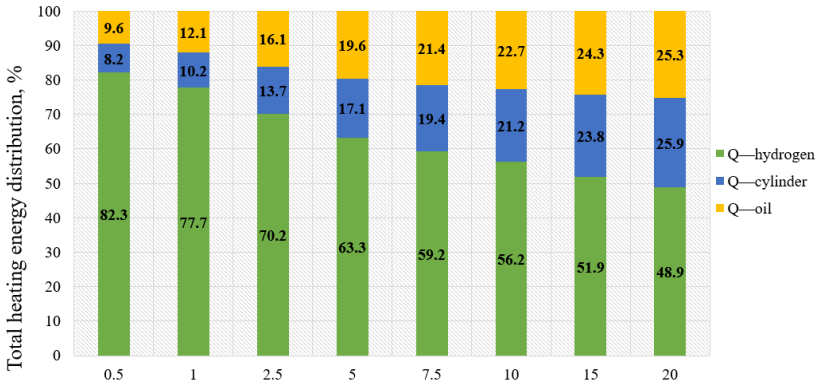

Figure 11. Diagrams of thermal energy distribution Q_T between energies accumulated in hydrogen Q_H, oil Q_F, and compression cylinder body Q_C for different durations of the compression stroke t_s at initial pressures P_1 = 3.0 MPa and compression ratio K_c = 5.0.

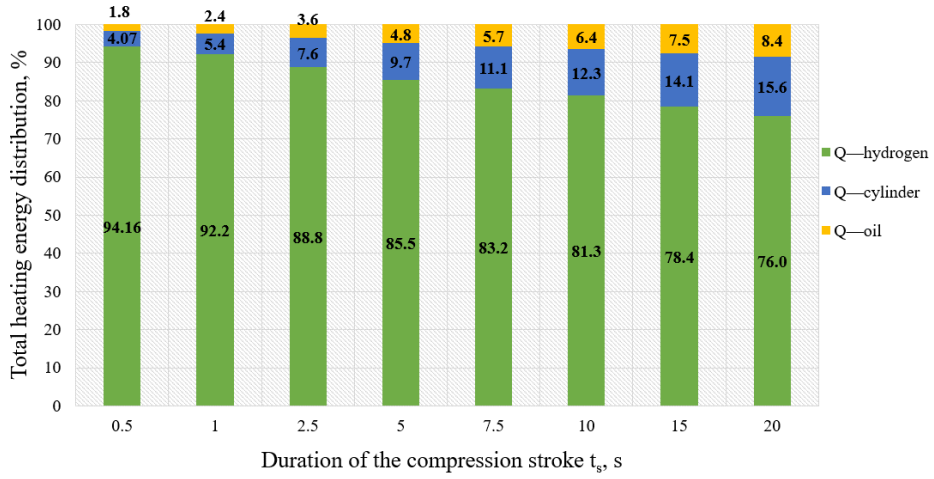

Figure 12. Diagrams of thermal energy distribution Q_T between energies accumulated in hydrogen Q_H, oil Q_F, and compression cylinder body Q_C for different durations of the compression stroke t_s at initial pressures P_1 = 20.0 MPa and compression ratio K_c = 5.0.

Figure 12 illustrates the distribution of the thermal energy among the hydrogen gas, liquid piston, and metal walls during the compression process. As expected, the metal walls absorb more heat than the liquid piston, given the geometry of the chamber, where three walls are metal and only one is in direct contact with the liquid. This result aligns with the physical arrangement of the system and supports the conclusions by providing a quantitative comparison of heat distribution.

The figure reinforces the significant role of the metal walls in dissipating heat during compression, underscoring the importance of their thermal properties in optimizing the system's cooling efficiency. While these findings are consistent with expectations, they highlight the need to focus on improving the heat dissipation capacity of the metal walls, which could involve enhancing their surface area or using materials with higher thermal conductivity.

In real conditions, hydrogen and oil inside the cylinder are constantly being mixed and exchanging energy. In this case, it is fair to assume that once hydrogen and oil are mixed, the temperature of the medium inside the compression chamber averages out, cooling the gas and increasing the temperature of the oil.

To compare different compression scenarios, including stroke duration, initial pressure, and cylinder geometry, the overall temperature of the system ΔT_O, equivalent to the energy consumed for hydrogen compression, is employed. The overall temperature ΔT_O is defined as follows:

$$\Delta T_O = (Q_F + Q_H + Q_C)/(m_F c_F + m_H c_H + m_C\, c_C) \quad (13)$$

where Q_F, m_F, c_F; Q_H, m_H, c_H; Q_C, m_C, c_C represent the energy, mass, and heat capacity of the work fluid, compressed hydrogen, and cylinder steel, respectively.

The changes of the ΔT_O for the different durations of compression stroke t_s at initial pressures P_1 = 3.0, 10.0, 15.0, and 20.0 MPa and compression ratio K_c = 5.0 are shown in Figure 13. As the pressure in the compression chamber increases, the ΔT_O increases proportionally, as can be seen by comparing the curves for an initial pressure from 3.0 MPa to 20.0 MPa. The temperature ΔT_O inside the compression chamber slightly increases with increasing compression stroke duration and mainly depends on the initial pressure.

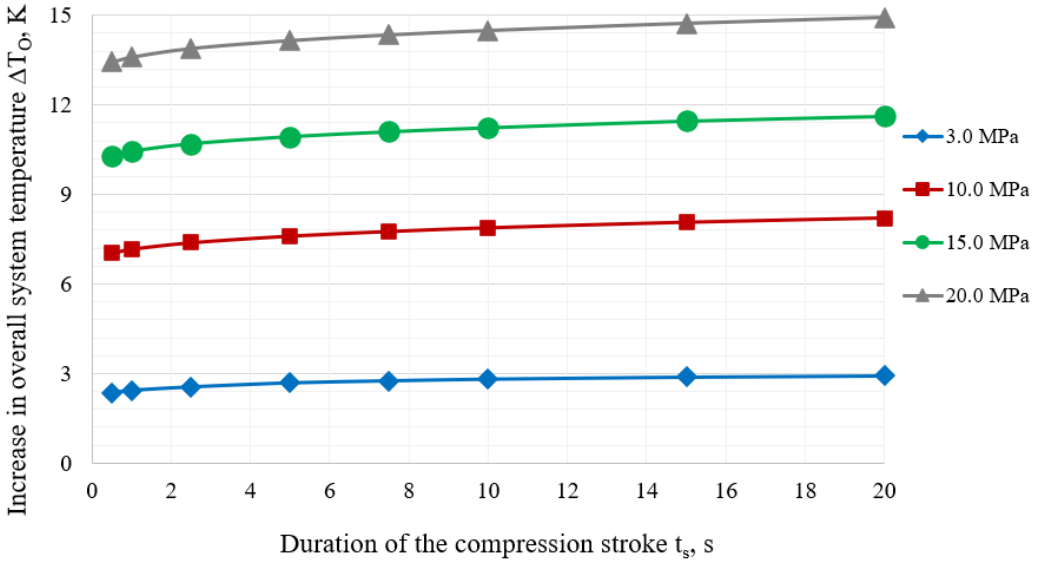

Figure 13. Increase in overall system temperature ΔT_O for different durations of the compression stroke t_s, at initial pressures P_1 = 3.0, 10.0, 15.0, and 20.0 MPa and compression ratio K_c = 5.0.

However, for the considered compression pressures, the overall temperature value is within the range of less than 15.0 K. This means that the temperature conditions inside the compression chamber should not exceed the temperature limits defined as rated values for the oil.

It is reasonable to assume that the actual hydrogen pressure will be 5 to 10% higher than obtained by Equation (2). This estimate is based on practical observations and findings from similar systems reported in the literature. It accounts for factors such as the potential mixing of liquid and gas inside the compression chamber, which can lead to localized pressure variations beyond those predicted by the idealized numerical model. Additionally, transient pressure spikes during the compression process, which were not explicitly modeled in this study, are known to occur in operational systems [61,62].

To manage the compression process effectively and control the pressure rise, intensive cooling is required at the top of the cylinder, as this region experiences the most significant rise in hydrogen temperature, as shown in Figure 6.

The analysis of the energy required to perform a hydrogen compression stroke with a given compression ratio makes it possible to estimate the power of the liquid pump drive motor required to perform this work in a given time. As a first approximation, the value of this power can be determined from the following:

$$W = Q_T / t_s \tag{14}$$

The curves of total power W for the examined models are presented in Figure 14, where power is calculated as a function of the duration of compression stroke t_s, at initial pressures P_1 = 3.0, 10.0, 15.0, and 20.0 MPa and the compression ratio K_c = 5.0.

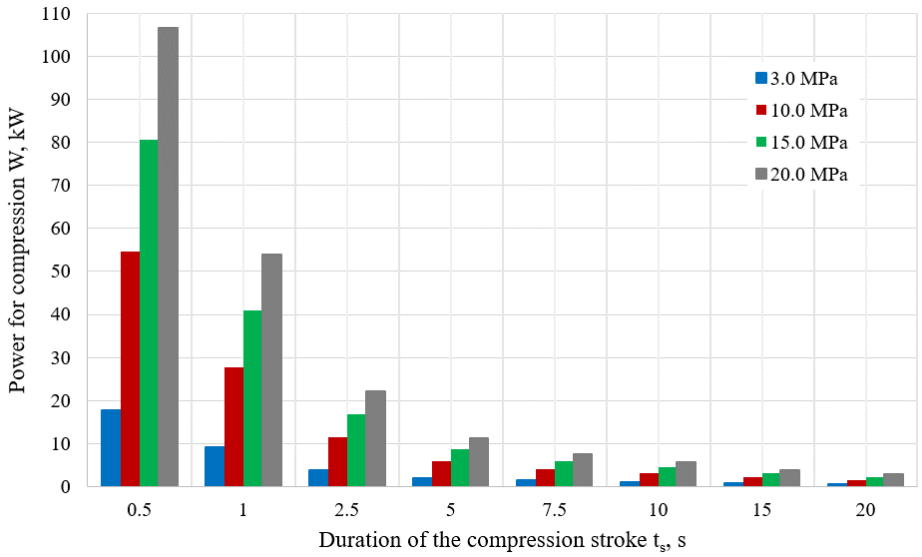

Figure 14. The power W required for hydrogen compression for different durations of the compression stroke t_s at initial pressures P_1 = 3.0, 10.0, 15.0, and 20.0 MPa and compression ratio K_c = 5.0.

Figure 14 illustrates the relationship between the power required for compression and the duration of the compression stroke for four different initial hydrogen pressures. As the duration of the compression stroke increases, the power required for compression decreases significantly across all pressure levels. This indicates that longer compression strokes distribute the work over a longer period, resulting in a reduction in the instantaneous power demand. At any given duration, the power required is higher for higher initial hydrogen pressures. For example, at the shortest duration, 20.0 MPa requires significantly more power than 3.0 MPa, highlighting the increased energy demand at higher pressures. However, it is important to note that these power values correspond to different flow rates. Longer compression strokes handle a lower hydrogen flow rate, while shorter strokes allow for higher flow rates. To match the flow rate of shorter cycle times with longer strokes, additional pumps or compression units may be required, potentially increasing system complexity and cost. This trade-off must be considered when designing systems for high-throughput applications.

The power drop is most notable in the shorter stroke durations, after which the reduction in power becomes more gradual. While extending the compression stroke duration can be a viable strategy to minimize the power rating of individual pumps, the overall system efficiency must account for the number of pumps required to maintain the equivalent throughput.

5. Conclusions

This study provides an in-depth analysis of the thermodynamic processes involved in hydraulic hydrogen compression using numerical simulations developed in COMSOL Multiphysics®. The findings reveal important insights that can be leveraged to optimize the design, efficiency, and energy consumption of hydraulic hydrogen compression systems, particularly in high-pressure applications such as refueling stations.

One significant finding is the temperature distribution within the compression chamber. The numerical model demonstrates that while initial heat generation occurs near the molecules compressed by the liquid piston, the upper part of the chamber retains the most heat as the compression progresses. This is attributed to the gas in this region being farther from the immediate cooling effect of the liquid piston, leading to less efficient heat dissipation. Effective thermal management in this region, particularly through optimized cooling systems, such as a closed-top chamber design and enhanced external cooling mechanisms, is essential to prevent overheating and ensure stable operation.

The study highlights the interplay between the liquid piston and the chamber design in managing heat. The liquid piston facilitates rapid heat transfer by absorbing heat from the compressed gas and transferring it to the chamber walls, while the closed-top design enhances external heat dissipation. This synergy underscores the importance of integrating these design elements to optimize system performance.

For practical applications, longer stroke durations of 15–20 s are recommended due to their lower instantaneous power requirements, enabling the use of smaller, less expensive pumps. These durations are ideal for systems where throughput is not the primary constraint. Initial hydrogen pressures around 10 MPa offer a balance between manageable temperature increases and reasonable energy requirements during compression, reducing the risk of excessive heating while maintaining efficiency in hydrogen refueling scenarios.

The integration of the calculations with simulations strengthens the study's findings by ensuring the numerical model's reliability through well-defined initial parameters and boundary conditions aligned with physical principles. Additionally, the calculations provide quantitative insights into energy distribution and the impact of compression stroke duration on power consumption, enhancing the understanding of system performance.

The use of the superposition method in the numerical model proved effective for simplifying the calculations while maintaining precision in predicting the temperature and energy distributions. This approach offers valuable insights into the thermodynamic interactions between hydrogen, oil, and cylinder walls, enabling further system optimization.

The simulations revealed that increasing the initial hydrogen pressure leads to higher chamber temperatures and greater energy requirements. Understanding the energy distribution among hydrogen, oil, and chamber walls allows for more accurate performance predictions and informs strategies for optimizing cooling and improving system efficiency.

This study focuses on a single compression stroke and does not account for the thermal effects of repeated cycles, such as heat accumulation in the walls and liquid over time. Future research should address multi-cycle simulations to capture these cumulative effects and develop a more comprehensive understanding of operational performance. Additionally, exploring alternative oils with improved thermal properties and enhancing cooling mechanisms could further improve system performance and reliability.

These findings contribute to the development of more efficient hydraulic hydrogen compression systems, particularly for refueling station applications where energy consumption, thermal management, and system scalability are critical.

Author Contributions: Conceptualization, V.B. (Valerijs Bezrukovs) and V.B. (Vladislavs Bezrukovs); methodology, V.B. (Valerijs Bezrukovs), D.B., and I.K.; software, I.K.; validation, V.B. (Valerijs Bezrukovs), V.B. (Vladislavs Bezrukovs), and M.K.; formal analysis, V.B. (Valerijs Bezrukovs); investigation, V.B. (Valerijs Bezrukovs); resources, M.K.; data curation, A.I.P.; writing—original draft preparation, M.K.; writing—review and editing, M.K. and A.I.P.; visualization, M.K. and D.B.; supervision, V.B. (Valerijs Bezrukovs); project administration, V.B. (Vladislavs Bezrukovs); funding acquisition, V.B. (Valerijs Bezrukovs). All authors have read and agreed to the published version of the manuscript.

Funding: The research has been financed by ERDF project "Experimental Studies and Development of Technology on Hydraulic Compression of Hydrogen", No. 1.1.1.1/20/A/185, implemented at the Ventspils University of Applied Sciences.

Institutional Review Board Statement: Not applicable.

Informed Consent Statement: Not applicable.

Data Availability Statement: In order to obtain access to more information about the model used in this research, the reader can contact the corresponding author.

Acknowledgments: This research has been supported by the HORIZON Coordination and Support Action project MarTe: Marine Technology Excellence Hub for Sustainable Blue Economy in the Baltics, project ID: 101186498. We extend our sincere gratitude to the Process Analysis and Research Centre (PAIC), Ltd., for their invaluable assistance with COMSOL modeling.

Conflicts of Interest: The authors declare no conflicts of interest.

References

1. Hoffmann, P. *Tomorrow's Energy, Revised and Expanded Edition: Hydrogen, Fuel Cells, and the Prospects for a Cleaner Planet*; MIT Press: Cambridge, MA, USA, 2012.
2. Lah, O. Decarbonizing the transportation sector: Policy options, synergies, and institutions to deliver on a low-carbon stabilization pathway. *Wiley Interdiscip. Rev. Energy Environ.* **2017**, *6*, e257. [CrossRef]
3. Hassanpouryouzband, A.; Wilkinson, M.; Haszeldine, R.S. Hydrogen energy futures–foraging or farming? *Chem. Soc. Rev.* **2024**, *53*, 2258–2263. [CrossRef]
4. European Commission. A Hydrogen Strategy for a Climate-Neutral Europe. Communication from the Commission to the European Parliament, the Council, the European Economic and Social Committee and the Committee of the Regions. Brussels, 8 July 2020. COM (2020) 301 Final. Available online: https://www.eumonitor.eu/9353000/1/j9vvik7m1c3gyxp/vla6qbjzcok1 (accessed on 15 December 2024).
5. Reda, B.; Elzamar, A.A.; AlFazzani, S.; Ezzat, S.M. Green hydrogen as a source of renewable energy: A step towards sustainability, an overview. *Environ. Dev. Sustain.* **2024**, 1–21. [CrossRef]
6. Osman, A.I.; Mehta, N.; Elgarahy, A.M.; Hefny, M.; Al-Hinai, A.; Al-Muhtaseb, A.A.H.; Rooney, D.W. Hydrogen production, storage, utilisation and environmental impacts: A review. *Environ. Chem. Lett.* **2022**, *20*, 153–188. [CrossRef]
7. Singla, M.K.; Nijhawan, P.; Oberoi, A.S. Hydrogen fuel and fuel cell technology for cleaner future: A review. *Environ. Sci. Pollut. Res.* **2021**, *28*, 15607–15626. [CrossRef] [PubMed]
8. Zhang, D.; Jiang, M.; Li, G.; Tang, Y. An advanced bibliometric analysis and future research insights on safety of hydrogen energy. *J. Energy Storage* **2024**, *77*, 109833. [CrossRef]
9. Cui, G.; Li, Y.; Wu, D.; Li, H.; Liu, H.; Xing, X.; Liu, J. The Progress of Autoignition of High-Pressure Hydrogen Gas Leakage: A Comprehensive Review. *Fire* **2024**, *7*, 268. [CrossRef]
10. Sattar, M.A.; Rasul, M.G.; Jahirul, M.I.; Hasan, M.M. An up-to-date review on the progress and challenges of hydrogen storage, and its safety and economic analysis. *Sustain. Energy Fuels* **2024**, *8*, 3545–3573. [CrossRef]
11. Qureshi, F.; Yusuf, M.; Khan, M.A.; Ibrahim, H.; Ekeoma, B.C.; Kamyab, H.; Rahman, M.M.; Nadda, A.K.; Chelliapan, S. A State-of-The-Art Review on the Latest trends in Hydrogen production, storage, and transportation techniques. *Fuel* **2023**, *340*, 127574. [CrossRef]
12. Widera, B. Renewable hydrogen implementations for combined energy storage, transportation and stationary applications. *Therm. Sci. Eng. Prog.* **2020**, *16*, 100460. [CrossRef]
13. Züttel, A. Materials for hydrogen storage. *Mater. Today* **2003**, *6*, 24–33. [CrossRef]
14. Ali, M.S.; Khan, M.S.H.; Tuhin, R.A.; Kabir, M.A.; Azad, A.K.; Farrok, O. Hydrogen energy storage and transportation challenges: A review of recent advances. *Hydrog. Energy Convers. Manag.* **2024**, 255–287.
15. Kamran, M.; Turzyński, M. Exploring hydrogen energy systems: A comprehensive review of technologies, ap-plications, prevailing trends, and associated challenges. *J. Energy Storage* **2024**, *96*, 112601. [CrossRef]
16. Le, T.T.; Sharma, P.; Bora, B.J.; Tran, V.D.; Truong, T.H.; Le, H.C.; Nguyen, P.Q.P. Fueling the future: A comprehensive review of hydrogen energy systems and their challenges. *Int. J. Hydrogen Energy* **2024**, *54*, 791–816. [CrossRef]

17. Halder, P.; Babaie, M.; Salek, F.; Haque, N.; Savage, R.; Stevanovic, S.; Bodisco, T.A.; Zare, A. Advancements in hydrogen production, storage, distribution and refuelling for a sustainable transport sector: Hydrogen fuel cell vehicles. *Int. J. Hydrogen Energy* **2024**, *52*, 973–1004. [CrossRef]
18. Hassan, Q.; Azzawi, I.D.; Sameen, A.Z.; Salman, H.M. Hydrogen fuel cell vehicles: Opportunities and challenges. *Sustainability* **2023**, *15*, 11501. [CrossRef]
19. Soleimani, A.; Hosseini Dolatabadi, S.H.; Heidari, M.; Pinnarelli, A.; Mehdizadeh Khorrami, B.; Luo, Y.; Vizza, P.; Brusco, G. Progress in hydrogen fuel cell vehicles and up-and-coming technologies for eco-friendly transportation: An inter-national assessment. *Multiscale Multidiscip. Model. Exp. Des.* **2024**, *7*, 3153–3172. [CrossRef]
20. Thomas, C.E. Fuel cell and battery electric vehicles compared. *Int. J. Hydrogen Energy* **2009**, *34*, 6005–6020. [CrossRef]
21. Ziyu, L.; Yan, W. Hydrogen Refueling Station Siting and Development Planning in the Delivery Industry. In *Resilient and Adaptive Tokyo: Towards Sustainable Urbanization in Perspective of Food-Energy-Water Nexus*; Springer Nature: Singapore, 2024; pp. 231–251.
22. Bhogilla, S.S.; Niyas, H. Design of a hydrogen compressor for hydrogen fueling stations. *Int. J. Hydrogen Energy* **2019**, *44*, 29329–29337. [CrossRef]
23. Lundblad, T.; Taljegard, M.; Johnsson, F. Centralized and decentralized electrolysis-based hydrogen supply systems for road transportation–A modeling study of current and future costs. *Int. J. Hydrogen Energy* **2023**, *48*, 4830–4844. [CrossRef]
24. Lahnaoui, A.; Wulf, C.; Heinrichs, H.; Dalmazzone, D. Optimizing hydrogen transportation system for mobility by minimizing the cost of transportation via compressed gas truck in North Rhine-Westphalia. *Appl. Energy* **2018**, *223*, 317–328. [CrossRef]
25. Pandey, A.P. Recent Progress and Challenges in Hydrogen Storage Medium and Transportation for Boosting Hydrogen Economy Anant Prakash Pandey, Vijay K. Singh, and Ambesh Dixit. *Energy Mater. Devices Proc.* **2024**, *2022*, 183.
26. Bezrukovs, V.; Bezrukovs, V.; Konuhova, M.; Bezrukovs, D.; Kaldre, I.; Berzins, A. R&D of a Hydraulic Hydrogen Compression System for Refuelling Stations. *Latv. J. Phys. Tech. Sci.* **2023**, *60*, 21–39.
27. Yu, M.; Wang, K.; Vredenburg, H. Insights into low-carbon hydrogen production methods: Green, blue and aqua hydrogen. *Int. J. Hydrogen Energy* **2021**, *46*, 21261–21273. [CrossRef]
28. Ma, N.; Zhao, W.; Wang, W.; Li, X.; Zhou, H. Large scale of green hydrogen storage: Opportunities and challenges. *Int. J. Hydrogen Energy* **2024**, *50*, 379–396. [CrossRef]
29. Kourougianni, F.; Arsalis, A.; Olympios, A.V.; Yiasoumas, G.; Konstantinou, C.; Papanastasiou, P.; Georghiou, G.E. A comprehensive review of green hydrogen energy systems. *Renew. Energy* **2024**, *231*, 120911. [CrossRef]
30. Sebbagh, T.; Şahin, M.E.; Beldjaatit, C. Green hydrogen revolution for a sustainable energy future. *Clean Technol. Environ. Policy* **2024**, *26*, 4017–4040. [CrossRef]
31. Wang, T.; Cao, X.; Jiao, L. PEM water electrolysis for hydrogen production: Fundamentals, advances, and pro-spects. *Carbon Neutrality* **2022**, *1*, 21. [CrossRef]
32. Sdanghi, G.; Maranzana, G.; Celzard, A.; Fierro, V. Review of the current technologies and performances of hydrogen compression for stationary and automotive applications. *Renew. Sustain. Energy Rev.* **2019**, *102*, 150–170. [CrossRef]
33. Jia, G.; Cai, M.; Xu, W.; Shi, Y. Energy conversion characteristics of reciprocating piston quasi-isothermal com-pression systems using water sprays. *Sci. China Technol. Sci.* **2018**, *61*, 285–298. [CrossRef]
34. Specklin, M.; Deligant, M.; Sapin, P.; Solis, M.; Wagner, M.; Markides, C.N.; Bakir, F. Numerical study of a liquid-piston compressor system for hydrogen applications. *Appl. Therm. Eng.* **2022**, *216*, 118946. [CrossRef]
35. Platzer, M.F.; Sarigul-Klijn, N. Hydrogen Compression Technology. In *The Green Energy Ship Concept*; Spring-erBriefs in Applied Sciences and Technology; Springer: Cham, Switzerland, 2021.
36. Bezrukovs, V.; Bezrukovs, V.; Konuhova, M.; Bezrukovs, D.; Berzins, A. Hydrogen hydraulic compression system for refuelling stations. *Latv. J. Phys. Tech. Sci.* **2022**, *59*, 96–105. [CrossRef]
37. Van de Ven, J.D.; Li, P.Y. Liquid piston gas compression. *Appl. Energy* **2009**, *86*, 2183–2191. [CrossRef]
38. Franco, A.; Giovannini, C. Hydrogen Gas Compression for Efficient Storage: Balancing Energy and Increasing Density. *Hydrogen* **2024**, *5*, 293–311. [CrossRef]
39. Specklina, M.; Deliganta, M.; Sapinb, P.; Solisa, M.; Wagnerc, M.; Markidesb, C.N.; Bakira, F. CFD study of a liquid-piston compressor system for hydrogen applications. *Preprints* **2022**.
40. Zhou, H.; Ooi, K.T.; Dong, P.; Yang, Z.; Zhou, S.; Zhao, S. Dynamic and energy analysis of a liquid piston hydrogen compressor. *Int. J. Hydrogen Energy* **2023**, *48*, 20694–20704. [CrossRef]
41. Huynh, V.T.; Kim, D. Numerical investigations of heat transfer enhancement in ionic liquid-piston compressor using cooling pipes. *J. Vis.* **2024**, 1–23. [CrossRef]
42. Patil, V.C.; Liu, J.; Ro, P.I. Efficiency improvement of liquid piston compressor using metal wire mesh for near-isothermal compressed air energy storage application. *J. Energy Storage* **2020**, *28*, 101226. [CrossRef]
43. Kermani, N.A.; Rokni, M. Heat Analysis of Liquid piston Compressor for Hydrogen Applications. In Proceedings of the 20th World Hydrogen Energy Conference 2014, Gwangju, Republic of Korea, 15–20 June 2014.
44. Gouda, E.M.; Fan, Y.; Benaouicha, M.; Neu, T.; Luo, L. Review on Liquid Piston technology for compressed air energy storage. *J. Energy Storage* **2021**, *43*, 103111. [CrossRef]
45. Kermani, N.A.; Rokni, M. Heat transfer analysis of liquid piston compressor for hydrogen applications. *Int. J. Hydrogen Energy* **2015**, *40*, 11522–11529. [CrossRef]

46. Patil, V.C.; Acharya, P.; Ro, P.I. Experimental investigation of heat transfer in liquid piston compressor. *Appl. Therm. Eng.* **2019**, *146*, 169–179. [CrossRef]
47. Rouhi, S.; Sadeqi, S.; Xiros, N.; Ioup, J. CFD analysis of filling process for a hydrogen energy storage system. In Proceedings of the 5th Thermal and Fluids Engineering Conference (TFEC), New Orleans, LA, USA, 5–8 April 2020.
48. Rouhi, S.; Xiros, N.; Sadeqi, S.; Ioup, J.; Sultan, C.; Van Zwieten, J. CFD validation of the thermodynamic model of a compressed gaseous hydrogen storage tank. In Proceedings of the 5–6th Thermal and Fluids Engineering Conference (TFEC), New Orleans, LA, USA, 26–28 May 2021.
49. Wieberdink, J.; Li, P.Y.; Simon, T.W.; Van de Ven, J.D. Effects of porous media insert on the efficiency and power density of a high pressure (210 bar) liquid piston air compressor/expander–An experimental study. *Appl. Energy* **2018**, *212*, 1025–1037. [CrossRef]
50. Zhou, H.; Dong, P.; Zhao, S.; Geng, M.; Guo, Y.; Wang, Y. Interrupted plate porous media design for ionic liquid-type liquid piston hydrogen compressor and analysis of the effect on compression efficiency. *J. Energy Storage* **2022**, *51*, 104410. [CrossRef]
51. Bezrukovs, V.; Bezrukovs, V.; Bezrukovs, D.; Orlova, S.; Konuhova, M.; Berzins, A.; Kadakovskis, J.; Pranskus, P. Hydrogen Hydraulic Compression Device. WO2023017306, 16 March 2023.
52. Bezrukovs, V.; Bezrukovs, V.; Bezrukovs, D.; Konuhova, M.; Berzins, A. For Hydraulic Compression of Hydrogen with Limited Foam Formation in the Working Fluid. LV15782, 20 April 2024.
53. Bezrukovs, V.; Bezrukovs, V.; Bezrukovs, D.; Konuhova, M.; Berzins, A. Hydrogen Hydraulic Compression Device. European Patent Application No. EP4352368A1, 17 April 2024.
54. Kang, X.; Gao, X.; Liu, Z.; Cai, L.; Li, Y. Modeling and development of a liquid piston hydrogen compressor with a double buffer structure: A new insight. *Int. J. Hydrogen Energy* **2023**, *48*, 12410–12423. [CrossRef]
55. Ye, J.; Du, Z.; Xie, J.; Yin, X.; Peng, W.; Yan, Z. Transient flow performance and heat transfer characteristic in the cylinder of hydraulic driving piston hydrogen compressor during compression stroke. *Int. J. Hydrogen Energy* **2023**, *48*, 7072–7084. [CrossRef]
56. Linstrom, P.J.; Mallard, W.G. The NIST Chemistry WebBook: A chemical data resource on the internet. *J. Chem. Eng. Data* **2001**, *46*, 1059–1063. [CrossRef]
57. COMSOL AB, *COMSOL Multiphysics® Material Library*; Version 6.1; COMSOL AB: Stockholm, Sweden, 2024; [Online]; Available online: https://www.comsol.com/ (accessed on 15 December 2024).
58. Gkanas, E.I.; Makridis, S.S.; Stubos, A.K. Three–Stage Hydrogen Compression System. Simulating Study with Comsol Multiphysics. In Proceedings of the 2012 COMSOL Conference, Milan, Italy, 10–12 October 2012.
59. Chabane, D.; Serairi, L.; Iqbal, M.; Djerdir, A.; Fenineche, N.; Elkedim, O. Innovative method to estimate state of charge of the hydride hydrogen tank: Application of fuel cell electric vehicles. *Int. J. Model. Simul.* **2022**, *42*, 305–318. [CrossRef]
60. Tabatabaian, M. CFD module. In *Mercury Learning and Information*; Science British Columbia Institute of Technology: Burnaby, BC, Canada, 2015; 150p.
61. Ye, J.; Zhao, Z.; Zheng, J.; Salem, S.; Yu, J.; Cui, J.; Jiao, X. Transient flow characteristic of high-pressure hydrogen gas in check valve during the opening process. *Energies* **2020**, *13*, 4222. [CrossRef]
62. Guo, Y.; Tang, Y.; Cao, J.; Diao, A.; Peng, X. Control Strategies for Piston Trajectory in Ionic Compressors for Hydrogen Storage. *Appl. Sci.* **2023**, *13*, 11759. [CrossRef]